



Title	Hydrodynamic analysis of electron motion in the cathode fall using a Monte Carlo simulation
Author(s)	Dalvie, M.; Farouki, R. T.; Hamaguchi, S. et al.
Citation	Journal of Applied Physics. 1992, 72(7), p. 2620-2631
Version Type	VoR
URL	<a href="https://hdl.handle.net/11094/78513">https://hdl.handle.net/11094/78513</a>
rights	This article may be downloaded for personal use only. Any other use requires prior permission of the author and AIP Publishing. This article appeared in Journal of Applied Physics 72, 2620 (1992) and may be found at <a href="https://doi.org/10.1063/1.351562">https://doi.org/10.1063/1.351562</a> .
Note	

*The University of Osaka Institutional Knowledge Archive : OUKA*

<https://ir.library.osaka-u.ac.jp/>

The University of Osaka

# Hydrodynamic analysis of electron motion in the cathode fall using a Monte Carlo simulation

Cite as: Journal of Applied Physics **72**, 2620 (1992); <https://doi.org/10.1063/1.351562>

Submitted: 27 February 1992 . Accepted: 04 June 1992 . Published Online: 17 August 1998

M. Dalvie, R. T. Farouki, S. Hamaguchi, and M. Surendra



View Online



Export Citation



**New**

## Your Qubits. Measured.

Meet the next generation of quantum analyzers

- Readout for up to 64 qubits
- Operation at up to 8.5 GHz, mixer-calibration-free
- Signal optimization with minimal latency

[Find out more](#)



# Hydrodynamic analysis of electron motion in the cathode fall using a Monte Carlo simulation

M. Dalvie, R. T. Farouki, S. Hamaguchi, and M. Surendra

IBM Thomas J. Watson Research Center, P. O. Box 218, Yorktown Heights, New York 10598

(Received 27 February 1992; accepted for publication 4 June 1992)

The exact mass, momentum, and energy conservation equations for electron transport in a dc glow are derived from the Boltzmann equation. A Monte Carlo particle simulation is used to explicitly calculate the individual terms of the moment equations, and to gain insight into the behavior of the electron distribution function (EDF) moments such as density and average velocity. Pure forward scattering and isotropic scattering are considered as two limiting scattering mechanisms. When forward scattered, the electron fluid shows the maximum change in properties and in transport mechanisms at the field transition point between the cathode fall (CF) and the negative glow. Isotropic scattering, however, results in property changes a short distance inside the sheath. Diffusion of the low-energy, high-density, bulk plasma electrons into the CF causes dilution of the low-density, high-energy beam from the CF before the beam actually arrives at the low-field region. The applicability of commonly used closure relations which yield a fluid description of the system is evaluated. Use of fluid equations to characterize this system with no *a priori* knowledge of the EDF is limited by kinetic effects, such as heat flow against the temperature gradient, especially in the forward-scattered case where the EDF is very anisotropic. The description of inelastic rates by Arrhenius kinetics is found to be surprisingly accurate with both scattering mechanisms. However, while temperature is an adequate gauge of the characteristic energy under isotropic scattering, the energy of the bulk electron motion must be included under forward scattering. Also, Arrhenius kinetics sometimes produce a spurious double peak in the inelastic rate profile which is not reproduced by the Monte Carlo simulation. The anisotropy of the EDF under the forward-scatter assumption makes it difficult to justify the use of the mobility and heat conduction closure relations. Under isotropic scattering, however, electron inertia is negligible. In that case, under the discharge conditions used here, the drift-diffusion approximation to the flux is good to within a factor of 2. Classical heat conduction theory overestimates the heat flux by a factor of 4 at the sheath edge.

## I. INTRODUCTION

Glow discharge reactors are used routinely in the manufacture of integrated circuits. These discharges are characterized by nonequilibrium kinetics which makes them difficult to analyze. In recent years, a number of modeling efforts have attempted to explicitly account for the nonequilibrium character of these discharges by using particle methods<sup>1-3</sup> or by directly solving the Boltzmann equation.<sup>4</sup> However, these models have been restricted to one spatial dimension. The need for at least two-dimensional models of process tools is clear. Given the high computing costs of the aforementioned methods, fluid models of discharges<sup>5-8</sup> with some variations to accommodate nonequilibrium kinetics<sup>9-14</sup> appear more efficient.

This paper explores a hydrodynamic description of electrons in the nonequilibrium cathode fall (CF) of a dc glow discharge. The zeroth, first, and second moments of the Boltzmann equation (which give rise to the mass, momentum, and energy balance equations) are developed with no *a priori* assumption regarding the electron distribution function (EDF). We use a (Monte Carlo) particle simulation of the electron motion to calculate the EDF and each term in the Boltzmann moments.

The exercise allows us to gain fundamental understanding of electron motion in spatially varying electric

fields. Through the momentum and energy balances, it is possible to point to the dominating mechanisms of momentum and energy transport in the CF. Furthermore, by identifying the important terms in the balance equations, and appropriate approximations where necessary, it is possible to formulate a credible fluid model of electron motion in the CF.

## II. MODEL OF THE CATHODE FALL

Experimental measurements<sup>15</sup> and self-consistent simulations<sup>12,16,17</sup> indicate that the electric field in the CF is a linearly decreasing function of distance from the cathode. The model CF length is  $d=4$  mm, and the voltage  $V$  is 300 V. The discharge current density is set at  $2.0 \text{ A/m}^2$ , and we assume that the current is carried totally by electrons at the edge of the CF (to normalize the electron flux). The background gas pressure is set at 600 mTorr. The plasma or negative glow (NG) region is characterized by low electric fields, approximated here by a weakly positive constant field set at 1000 V/m (a positive field drives electrons from the cathode to the anode). Field reversals in the NG are ignored. The distance from the CF edge to the anode is fixed at 4 mm. The situation is shown schematically in Fig. 1. Similar field configurations have been used in previous simulations as well.<sup>15,18,19</sup>

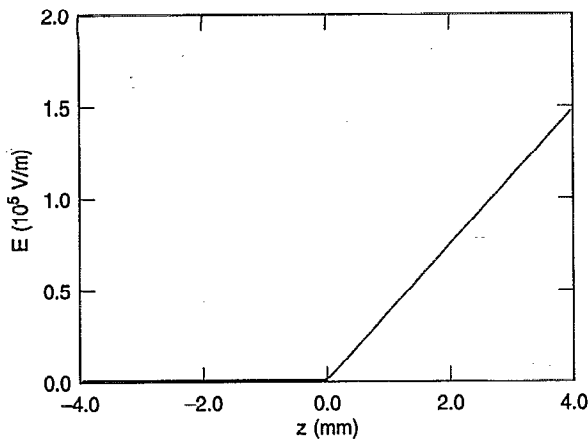


FIG. 1. Electric-field configuration used in simulation.  $d=4$  mm; cathode:  $z=d$ ; anode:  $z=-d$ ;  $V_{CF}=300$  V.

We use a simplified model of the CF in which electrons are emitted at the cathode by secondary processes. We use a Maxwellian distribution with a mean energy of 2 eV for the distribution of the emitted electrons. These electrons are accelerated by the high electric field adjacent to the cathode and soon attain energies higher than that required for excitation and ionization of neutral atoms. We include one excitation collision with a threshold of  $\phi_x=12$  eV and a constant cross section of  $1 \text{ \AA}^2$  above the threshold, and one ionization cross section with a threshold of  $\phi_i=18$  eV and a constant cross section of  $2 \text{ \AA}^2$  above the threshold. The numbers are chosen to reflect the properties of argon, although energy dependence beyond the threshold behavior has been ignored in the interest of simplicity. We have shown in a previous paper<sup>17</sup> that, notwithstanding the crudity of the collision models, we reproduce qualitatively all CF features shown in previous works using realistic cross sections. The simple cross sections used here allow us to analytically evaluate the Boltzmann collision integrals. We explore the effect of angular scattering by comparing two extreme cases, pure forward scattering and isotropic scattering. In the latter case, we also include elastic collisions with an energy-independent cross section of  $5 \text{ \AA}^2$ .

Details of the implementation of the model in the

$$\left(\frac{\delta f}{\delta t}\right)_e + \left(\frac{\delta f}{\delta t}\right)_x = \iint F(\mathbf{V}')f(\mathbf{v}')\|\mathbf{v}'-\mathbf{V}'\|\frac{\partial(\mathbf{v}')}{\partial(\mathbf{v})}[\sigma_e(\|\mathbf{v}'-\mathbf{V}'\|,\psi) + \sigma_x(\|\mathbf{v}'-\mathbf{V}'\|,\psi)]d^2\Omega d^3\mathbf{V}' - \iint F(\mathbf{V})f(\mathbf{v})\|\mathbf{v}-\mathbf{V}\|[\sigma_e(\|\mathbf{v}-\mathbf{V}\|,\psi) + \sigma_x(\|\mathbf{v}-\mathbf{V}\|,\psi)]d^2\Omega d^3\mathbf{V}, \quad (6)$$

where  $F(\mathbf{V})$  is the neutral distribution function,  $\mathbf{V}$  is the neutral velocity, and the primes indicate velocities before collisions. In Eq. (6) and those to follow, the  $z$  dependence of  $f$  is not explicitly stated. For this analysis, we assume that the neutrals are at rest and therefore the neutral distribution is given by

Monte Carlo program may be found in Ref. 17, with the important difference that this work is not self-consistent but uses a linear electric-field approximation.

### III. BOLTZMANN EQUATION MOMENTS

Before commencing, we define the the distribution function for electrons,

$$dn = f(\mathbf{v},z)d^3\mathbf{v}, \quad (1)$$

where  $dn$  is the differential density of electrons at  $z$  with velocities in  $d^3\mathbf{v}$ ,  $f(\mathbf{v},z)$  is the distribution function,  $\mathbf{v}$  is the electron velocity, and  $z$  is defined on a coordinate axis parallel to the electric field. The geometry is assumed to be plane parallel, implying an axisymmetric distribution function which we write as

$$f(\mathbf{v},z) = f(v_z, v_\perp, z), \quad (2)$$

where  $v_z, v_\perp$  are the axial and perpendicular components of the velocity vector ( $v_\perp = \sqrt{v_x^2 + v_y^2}$ ).

We are interested in the steady-state behavior of the CF for which we may begin with the time-independent Boltzmann equation,

$$\mathbf{v}\cdot\nabla_x f + \mathbf{a}\cdot\nabla_v f = \left(\frac{\delta f}{\delta t}\right)_{\text{coll}}, \quad (3)$$

where  $\mathbf{a}$  is the acceleration of electrons due to the CF field. Axisymmetry reduces Eq. (3) to

$$v_z \frac{\partial f}{\partial z} - \frac{eE}{m} \frac{\partial f}{\partial v_z} = \left(\frac{\delta f}{\delta t}\right)_{\text{coll}}, \quad (4)$$

where  $m$  is the electronic mass,  $e$  is the unit charge, and  $E$  is the local electric field.

We write the collision integral as a sum of component collision integrals,

$$\left(\frac{\delta f}{\delta t}\right)_{\text{coll}} = \left(\frac{\delta f}{\delta t}\right)_e + \left(\frac{\delta f}{\delta t}\right)_x + \left(\frac{\delta f}{\delta t}\right)_i, \quad (5)$$

where the subscripts refer to elastic, excitation, and ionization, respectively. As stated above, elastic collisions are not considered in the pure forward scattering case [ $(\delta f/\delta t)_e = 0$ ]. The elastic and excitation components can be written as<sup>20</sup>

$$F(\mathbf{V}') = n_g \delta(\mathbf{V}'), \quad F(\mathbf{V}) = n_g \delta(\mathbf{V}), \quad (7)$$

where  $n_g$  is the neutral gas density. This assumption is justified for electron-neutral interactions since electron velocities are typically orders of magnitude higher than neu-

tral velocities. We proceed by incorporating Eq. (7) into Eq. (6) and integrating over the neutral velocity space to obtain

$$\begin{aligned} & \left(\frac{\delta f}{\delta t}\right)_e + \left(\frac{\delta f}{\delta t}\right)_x \\ &= \int n_g f(\mathbf{v}') v' \frac{\partial(\mathbf{v}')}{\partial(\mathbf{v})} [\sigma_e(v', \psi) + \sigma_x(v', \psi)] d^2\Omega \\ & - \int n_g f(\mathbf{v}) v [\sigma_e(v, \psi) + \sigma_x(v, \psi)] d^2\Omega, \end{aligned} \quad (8)$$

where  $v = \|\mathbf{v}\|$ .

Ionizing collisions are more complicated because of the production of a secondary electron with a variable energy  $\epsilon$ . The collision integral for this case is written as

$$\begin{aligned} \left(\frac{\delta f}{\delta t}\right)_i &= \iint n_g f(\mathbf{v}') v' \frac{\partial(\mathbf{v}')}{\partial(\mathbf{v})} \sigma_i^\epsilon(v', \epsilon, \psi) d\epsilon d^2\Omega \\ & - \iint n_g f(\mathbf{v}) v \sigma_i^\epsilon(v, \epsilon, \psi) d\epsilon d^2\Omega. \end{aligned} \quad (9)$$

Equation (9) incorporates Eq. (7) and the integration over the secondary energy  $\epsilon$  is done over the allowable range. The first integral on the right-hand side actually represents two integrals with different scattering maps relating  $\mathbf{v}'$  and  $\mathbf{v}$ , one each for primary and secondary electrons.

The continuity equation for the electrons is obtained by integrating Eqs. (4), (8), and (9) over the velocity space of the electrons  $d^3\mathbf{v}$ . In order to integrate the collision integrals, it is necessary to use<sup>20</sup>

$$\frac{\partial(\mathbf{v}')}{\partial(\mathbf{v})} d^3\mathbf{v} = d^3\mathbf{v}'. \quad (10)$$

As is well known, elastic and excitation collisions do not contribute to the zeroth moment [the right-hand side of Eq. (8) vanishes in the integration over  $d^3\mathbf{v}$ ]. The first integral on the right-hand side of Eq. (9) represents two separate integrals for primary and secondary electrons, as stated before. The integral over primary electrons is offset by the second integral in Eq. (9). There is therefore a net contribution to the zeroth moment from the integral over secondary electrons, as expected.

Defining the total ionization cross section as

$$\sigma_i \equiv \int_0^{\epsilon_i^x} \sigma_i^\epsilon d\epsilon, \quad (11)$$

where  $\epsilon_i^x = (mv'^2/2) - e\phi_i$  is the kinetic energy possessed by the electron in excess of the ionization potential  $\phi_p$  we can write the continuity equation as

$$\begin{aligned} \frac{d}{dz} (nu_z) &= \int \left(\frac{\delta f}{\delta t}\right)_i d^3\mathbf{v} \\ &= n_g \iint f(\mathbf{v}) v \sigma_i(v, \psi) d^2\Omega d^3\mathbf{v} \\ &= S_i, \end{aligned} \quad (12)$$

where  $u_z$  is the  $z$  component of the average velocity ( $u_z = \langle v_z \rangle$ ). Since the electric field points along the  $z$  direction, there is no perpendicular drift ( $u_\perp = 0$ ). In Eq. (12),  $S_i$  is the ionization rate (in units of  $\text{cm}^{-3} \text{s}^{-1}$ ). While  $\sigma_i$  is formally a function of the incoming velocity and the scattering angles of the primary and secondary electrons, we assume in this work that it is a constant.

The momentum balance is obtained from the Boltzmann equation by multiplying Eqs. (4), (8), and (9) by  $m\mathbf{v}$  before integrating over  $d^3\mathbf{v}$ . Following Ref. 21 we designate the integrals over the collision terms by  $mn\mathbf{R}$  with  $\mathbf{R}$  given by

$$\mathbf{R}(z) = -\frac{1}{n(z)} \int \mathbf{w} \left(\frac{\delta f}{\delta t}\right)_{\text{coll}} d^3\mathbf{v}, \quad (13)$$

where  $\mathbf{w}$  is the the random component of the velocity vector. Here,  $\mathbf{R}$  is the deceleration per electron due to collisions. The  $z$  component of the momentum balance can then be written as<sup>21</sup>

$$mnu_z \frac{du_z}{dz} + neE + \frac{dP_{zz}}{dz} + mnR_z = 0, \quad (14)$$

where use has been made of Eq. (12) and of the identity  $v_z \equiv u_z + w_z$ .

Evaluation of  $R_z$ , the dynamical friction term, is more convenient if Eq. (13) is rewritten as

$$R_z(z) = -\frac{1}{n} \int v_z \left(\frac{\delta f}{\delta t}\right)_{\text{coll}} d^3\mathbf{v} + \frac{u_z}{n} \int \left(\frac{\delta f}{\delta t}\right)_{\text{coll}} d^3\mathbf{v}. \quad (15)$$

As stated in the discussion preceding Eq. (12), integration of the collision integral [the second integrand in Eq. (15)] over velocity space yields the ionization rate  $S_i$ . Following Ref. 22, we write

$$R_z(z) = (R_{ez}^+ - R_{ez}^-) + (R_{iz}^+ - R_{iz}^-) + \frac{u_z S_i}{n} + (R_{xz}^+ - R_{xz}^-). \quad (16)$$

Here  $R_{ez}$ ,  $R_{iz}$ , and  $R_{xz}$  are the contributions to the first integral in Eq. (15) from the three component collision terms. A superscript  $+$  ( $-$ ) designates the contribution to each from the second (first) integrals in Eqs. (8) and (9). Physically,  $R^+$  may be construed as the momentum loss due to scattering out of the velocity element.  $R^-$  is the momentum gained by scattering into the velocity element. The extra ionization term is the inertia of the newly created electron, commonly called ionization drag. From Eqs. (8), (9), and (11), the  $R^+$  terms may be written as

$$R_{ez}^+ + R_{iz}^+ + R_{xz}^+ = n_g (\langle v_z v \sigma_e \rangle + \langle v_z v \sigma_i \rangle + \langle v_z v \sigma_x \rangle), \quad (17)$$

where all cross sections are total cross sections.

Evaluation of the integrals for  $R^-$ , however, requires knowledge of the scattering maps which relate the postcollision  $v_z$  and the precollision  $\mathbf{v}'$ . We use two extreme scattering models for the electrons, pure forward scattering and isotropic scattering. In the former, elastic collisions are ignored ( $R_{ez}^+ = R_{ez}^- = 0$ ). In ionization events, all allowed energy distributions between primary and secondary elec-

trons are equally probable. With these considerations, it is possible to show that for pure forward scattering the  $R^-$  terms are

$$R_{iz}^- = -n_g \langle \frac{4}{3} \sqrt{2\epsilon_i^x/mv\sigma_i} \rangle, \quad (18)$$

$$R_{xz}^- = -n_g \langle \sqrt{2\epsilon_x^x/mv\sigma_x} \rangle, \quad (19)$$

where  $\epsilon_i^x$  and  $\epsilon_x^x$  are the excess energy possessed by the electrons over the excitation and ionization thresholds, respectively. Note that in the forward-scattering case, the following conditions apply:  $v_1=0$ ,  $v_z < 0$ ,  $v = -v_x$ .

Combining Eqs. (16), (17), (18), and (19), the final form of the collision term for forward scattering is obtained,

$$mnR_z = mnn_g \langle (v_z + \frac{4}{3} \sqrt{2\epsilon_i^x/m})v\sigma_i \rangle + mu_z S_i + mnn_g \langle (v_z + \sqrt{2\epsilon_x^x/m})v\sigma_x \rangle. \quad (20)$$

For isotropic scattering, evaluation of  $R_{iz}^-$  and  $R_{xz}^-$  is simplified by assuming that the collisions are isotropic in the laboratory frame of reference. (Strictly, of course, this is not true but the small electron-neutral mass ratio justifies the assumption.) It is possible to show under this assumption that

$$R_{ez}^- = R_{iz}^- = R_{xz}^- = 0. \quad (21)$$

By Eq. (17) and (21), it is evident that the net effect of isotropic (in the laboratory frame) collisions is to destroy all gained momentum, which is expected. From Eqs. (16), (17), and (21), we write for isotropic scattering

$$mnR_z = mnn_g \langle (v_z v\sigma_e) + (v_z v\sigma_i) + (v_z v\sigma_x) \rangle + mu_z S_i. \quad (22)$$

For isotropic scattering, Eqs. (4) and (22) form the complete momentum balance equation for the average velocity  $u_z$ . For forward scattering, we replace Eq. (22) by Eq. (20).

It is well known about the Boltzmann equation that the system of equations derived by taking successively higher moments involve quantities in each equation which are determined by higher moments. Thus the continuity equation for the density, Eq. (12), involves the average velocity  $u_z$ , determined by Eq. (14). The higher-order term in Eq. (14) is the pressure term, which represents the transport of  $z$  momentum by random motion of the electrons in the  $z$  direction. The electron pressure  $P_{zz}$  is given by

$$P_{zz} = nm \langle w_z^2 \rangle \equiv nkT_z, \quad (23)$$

which defines the axial temperature  $T_z$ , and where  $k$  is the Boltzmann constant. The axial temperature is determined by the axial energy balance equation, which is derived by multiplying Eqs. (4), (8), and (9) by  $mv_z^2/2$  before integrating over velocity space. Incorporating Eq. (12), we write the rate of change of axial energy in a volume element of the electron fluid,<sup>21</sup>

$$0 = -neEu_z - nu_z \frac{d}{dz} (\frac{1}{2} mu_z^2 + \frac{1}{2} kT_z) - \frac{d}{dz} (P_{zz}u_z) - \frac{dq_z}{dz} - Q_z. \quad (24)$$

The first term represents Joule heating or  $j \cdot E$  (the Joule heating term as written is always positive in this system since the flux always follows the field, which indicates work done on the fluid element), the second term is the energy transport by convection, and the third term is the net rate of work done by pressure on the fluid element.<sup>23</sup> The quantity  $q_z$  is the "axial heat flux" due to random motion in the  $z$  direction defined as

$$q_z \equiv mn \langle w_z^3 \rangle / 2. \quad (25)$$

The collision integrals result in the term  $Q_z$ , given for forward scattering by

$$Q_z = (e\phi_i + \frac{1}{2} mu_z^2 + \frac{1}{2} kT_z) S_i + e\phi_x S_x, \quad (26)$$

and for isotropic scattering by

$$Q_z = \left( \frac{e\phi_i}{3} + \frac{1}{2} mu_z^2 + \frac{1}{2} kT_z \right) S_i + \frac{e\phi_x}{3} S_x - \frac{mnn_g}{2} \left\langle \left( \frac{v^2}{3} - v_z^2 \right) v (\sigma_e + \sigma_i + \sigma_x) \right\rangle. \quad (27)$$

Here we have ignored the energy lost to the neutral in an elastic (hard sphere) collision. Ionization loss includes the ionization potential of the neutrals as well as the energy required to bring newly created electrons from rest up to the average energy. The last term in Eq. (26) is the excitation loss ( $S_x$  is the excitation rate). The salient differences between Eqs. (26) and (27) are that the ionization and excitation losses are divided equally between the three coordinate directions (isotropic scattering), and the last term in Eq. (27) which represents the tendency towards an isotropic distribution due to collisions.

Since generally  $T_z \neq T_1$  under isotropic scattering, it is instructive to construct and analyze a second energy balance which determines the average temperature,  $T$ , defined as

$$3kT \equiv m \langle w^2 \rangle. \quad (28)$$

$T_1$  can then be obtained as  $T_1 = \frac{3}{2} T - \frac{1}{2} T_z$ . The total energy balance derived through a procedure similar to that used for Eq. (24) is written as

$$0 = -neEu_z - nu_z \frac{d}{dz} (\frac{1}{2} mu_z^2 + \frac{3}{2} kT) - \frac{d}{dz} (P_{zz}u_z) - \frac{dq}{dz} - Q, \quad (29)$$

where the new terms are  $q$ , the total heat flux,

$$q \equiv mn \langle w^2 w_z \rangle / 2, \quad (30)$$

and  $Q$ , the collisional heating,

$$Q = (e\phi_i + \frac{1}{2} mu_z^2 + \frac{3}{2} kT) S_i + e\phi_x S_x, \quad (31)$$

where the total random energy is written as  $\frac{3}{2}kT$  as opposed to  $\frac{1}{2}kT_z$  in Eq. (26) for forward scattering.

#### IV. CLOSURE RELATIONS

Fluid equations can be obtained from the moment equations (12), (14), (24), and (29) by the use of *ad hoc* closure relations. Previous fluid models of gas discharges have used various closure relations, depending upon whether the model was purely fluid<sup>5-8</sup> or a particle-fluid hybrid.<sup>9-14</sup> Our goal is to evaluate the various closure relations used to derive fluid models from Boltzmann moments. We restrict ourselves to relations used commonly in previous discharge models; the recent work of Kunhardt,<sup>24</sup> for example, on deriving closure relations for electron distributions in space-time varying fields is not considered. Unlike the models cited above, which include electron and ion transport and a self-consistent electric field, we study only electron transport.

The density of electrons is obtained by solving Eq. (12). It involves two unknown higher-order moments, the average velocity  $u_z$ , and the ionization rate  $S_i$ . The most accurate way to obtain the latter is through a particle-based Monte Carlo simulation with a few test particles in a specified field (the field is obtained from the fluid simulation). This method captures the nonequilibrium distribution of the "hot" electrons responsible for ionization (and excitation). Such an approach has been utilized recently in the modelling of dc glow discharges.<sup>9-14</sup>

An alternative method in which the EDF is assumed Maxwellian has also been used. Here the rate of reaction (ionization or excitation) can be written in the familiar Arrhenius form,

$$S^{Ar} = S^{\max} \exp(-e\phi/\bar{\epsilon}), \quad (32)$$

where  $S^{Ar}$  is the rate of the reaction (ionization or excitation),  $S^{\max}$  is the pre-exponential factor,  $\phi$  is the activation energy (ionization or excitation potential), and  $\bar{\epsilon}$  is the characteristic electron energy. For the cross sections used here, the pre-exponential factor is given by<sup>7</sup>

$$S^{\max} = nn_g \langle v \rangle \sigma_{\text{eff}} [1 + (e\phi/\bar{\epsilon})], \quad (33)$$

where  $\langle v \rangle$  is the average speed (for forward scattering only,  $\langle v \rangle = -u_z$ ), and  $\sigma_{\text{eff}}$  is the magnitude of the cross section above the threshold. Note that this approximation to the ionization rate requires the solution of the energy balance for the average energy (usually the temperature). The advantage of this approach over the particle simulation is that it involves the solution of fluid equations only. This has been used in Refs. 5 and 7.

It is also possible to assume that the EDF is in equilibrium with the local electric field, and calculate the ionization rate accordingly. In a recent 2D simulation of a dc glow, Boeuf<sup>8</sup> has made this approximation. This simplifies the fluid simulation since an energy balance is no longer required. However, Boeuf and Marode<sup>18</sup> and Gottscho *et al.*<sup>25</sup> have shown that equilibrium kinetics do not apply to the CF region. It is pointed out in Ref. 8 that this approximation limits the applicability of the model.

Along with the ionization rate, the average velocity must be specified to obtain the electron density through Eq. (12). This is obtained through the momentum balance [Eq. (14)], which involves two higher-order moments, the pressure  $P_{zz}$  and the dynamical friction term  $R_z$ . The pressure can be obtained by solving the energy balance equation for the temperature,<sup>5,7</sup> or by assuming that the electrons are isothermal.<sup>12</sup>

The friction term involves the complicated moments shown in Eqs. (20) and (22) which must be simplified in order to close the first moment. Based upon the magnitudes of the cross sections and the threshold behavior of the inelastic collision processes, it is usually assumed that electron momentum transfer due to collisions with neutrals is dominated by elastic collisions.<sup>7</sup> Since elastic scattering is ignored in the forward-scattering case, this simplification cannot be applied there. It may, however, be justified in the case of isotropic scattering. Beyond this assumption, further simplification of the friction term is necessary,<sup>7</sup>

$$mnR_z \approx mnn_g \langle v_z v \sigma_e \rangle \approx mnu_z \nu_e, \quad (34)$$

where  $\nu_e = n_g \langle \sigma_e v \rangle$  is the elastic collision frequency ( $\sigma_e$  is constant in this work). Besides the momentum loss due to scattering in inelastic collisions, the ionization drag has also been neglected in Eq. (34). Generally, this term is small compared to others in the frictional drag (except when inertial effects are very large, as in the forward-scattering case in the following section). Alternatively, it is possible to not fold the continuity equation into the first moment of the Boltzmann equation as was done in the derivation of Eq. (14), but rather to solve the equation in the form used by Meyyappan and Kreskovsky.<sup>7</sup>

Meyyappan and Kreskovsky<sup>7</sup> use the approximation above while solving the full momentum balance. It is more common to neglect electron inertia in Eq. (14) as well, which, when combined with Eq. (34) above, leads to the drift-diffusion equation,<sup>5</sup>

$$u_z = -\mu E - \frac{D}{P_{zz}} \frac{dP_{zz}}{dz}, \quad (35)$$

where  $\mu = e/m\nu_e$  is the electron mobility, and  $D = kT\mu/e$  is the electron diffusivity. Further simplifications of this equation have been made by assuming that mobility is constant, that  $T_z = T$ , and that the electrons are isothermal.<sup>8,12</sup>

For the constant elastic collision cross section used here, however, the mobility is not constant. Description of the mobility involves specification of the collision frequency  $\nu_e$ . Since the EDF is not known, it is usual to assume the electrons are Maxwell-Boltzmann distributed<sup>5,7</sup> in order to specify  $\nu_e$ . The mobility is then given by

$$\mu = \frac{e}{n_g \sigma_e} \left( \frac{\pi}{8mkT} \right)^{1/2}, \quad (36)$$

where we have included the assumption that the mobility is dominated by elastic collisions.

If the energy balance is solved (to obtain reaction rates through an Arrhenius description and to calculate the electron pressure), the second moment of the Boltzmann equation must be closed. The common practice is to assume

that  $T = T_z$  and solve the total energy balance.<sup>5,7</sup> Closing the total energy balance [Eq. (29)] requires, in addition to the closure relations discussed above, an expression for the heat flux. This is usually written as the heat conduction equation,<sup>5,7</sup>

$$q = -K \frac{dT}{dz}, \quad (37)$$

where  $K = \frac{3}{2} n k D$  is the electron thermal conductivity for particles near equilibrium undergoing hard-sphere interactions.<sup>23</sup>

We evaluate the effect of the closure relations in the succeeding sections. The fluid equations are not solved directly to make the comparison. Solution of the fluid equations needs, in addition to the closure relationships, specification of boundary conditions at the electrode. These are another source of discrepancy between results from fluid models and kinetic models since boundaries in kinetic descriptions (e.g., walls that absorb incident ions) may be approximated in more than one way in fluid models (e.g., by placing the condition on the density or the flux). Since the effects of boundary conditions are not restricted to the boundary region in general, a term-by-term comparison between a fluid solution and the Monte Carlo results would not provide any additional insight. Therefore, we extract the density and temperature (fluid properties) from the Monte Carlo (kinetic) simulation. These are then used to calculate terms used in the various closure relationships. Specifically, we compare Arrhenius rates to those obtained directly from the Monte Carlo simulation. The friction term calculated according to Eq. (34) is compared to that from the Monte Carlo simulation, which is the quantity on the right-hand side of Eq. (20) or (22). We also evaluate the validity of the drift-diffusion equation in the CF region. Finally, we compare the actual heat flux as calculated according to Eq. (37) with the flux from the simulation.

## V. FORWARD SCATTERING

Under the assumed field (Fig. 1), the gain in the electron current at the CF edge ( $z=0$ ) relative to the current emitted from the cathode ( $z=d$ ) is approximately 3.4. This is consistent with the mean free path for ionization,  $\lambda_i = 3$  mm, and the sheath thickness,  $d = 4$  mm. The value of  $\lambda_i$  is a lower bound because the threshold behavior is discounted. The gain calculated from this  $d/\lambda_i$  is  $e^{d/\lambda_i} = 3.8$  which is an upper limit. Of course, such a discussion is restricted to the pure forward-scattering case which is one dimensional in velocity space ( $v_{\perp} = 0$ ); angular scattering randomizes electron trajectories, making such analysis more difficult.

In Fig. 2, we show the density, the average velocity, the energy (total energy as well as the temperature), and the ionization rate. Comparing the plots in Fig. 2 with the field profile in Fig. 1 shows immediately that local equilibrium with the field is not attained anywhere in the discharge, a well-known feature.<sup>18</sup> The results shown are qualitatively consistent with previous results from the forward-scattering model used in Ref. 26. Briefly, the elec-

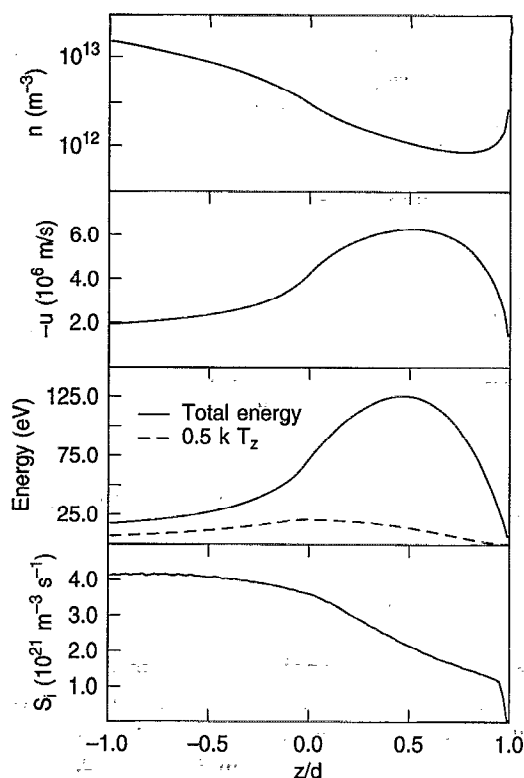


FIG. 2. Cathode fall properties using forward-scattering model.

trons pick up energy from the high field upon being emitted by the cathode ( $z=d$ ). This initial increase in the average velocity causes the drop in the electron density near the cathode. Ionization and excitation (not shown) begin once the electrons have gained sufficient energy to overcome the ionization potential barrier; from Fig. 2(d), this occurs very close to the cathode. The inelastic collision results in more electrons (increased density) being available for ionization. Ultimately, the decreasing field (or constant field in the NG) cannot replenish the energy loss in the inelastic collisions and the average energy [Fig. 2(c)] drops, causing the ionization (and excitation) rate to level off. From Fig. 2(c) it is clear that the temperature of the electrons is a small portion of the electron energy in the CF; the major portion of the average energy is the kinetic energy of the bulk motion.

To quantify the discussion above, we turn to the moment set derived for forward scattering in the previous section. The average velocity is determined by the momentum balance, and in Fig. 3 we show the four terms in Eq. (14) as a function of position. The interplay between the inertia term and the electric field is consistent with the above discussion, in that in the high-field region the electrons pick up momentum from the field which then drives the flow in the region where the field is low ( $z/d < 0.25$ ). In the low-field NG region ( $z < 0$ ), the resistance to the inertial force comes from frictional deceleration due to collisions and the pressure gradient. The large diffusive flux of electrons against the drift near the CF-NG boundary is

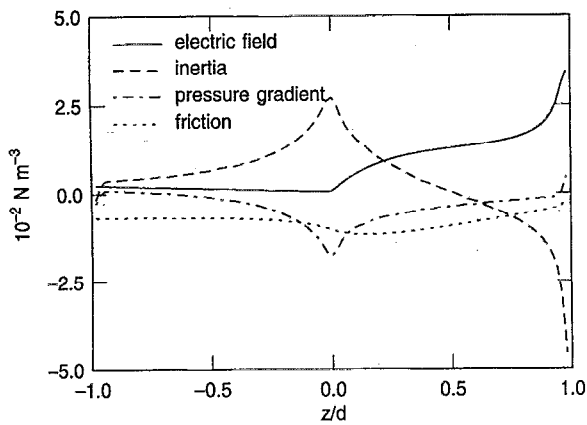


FIG. 3. Momentum balance with forward scattering.

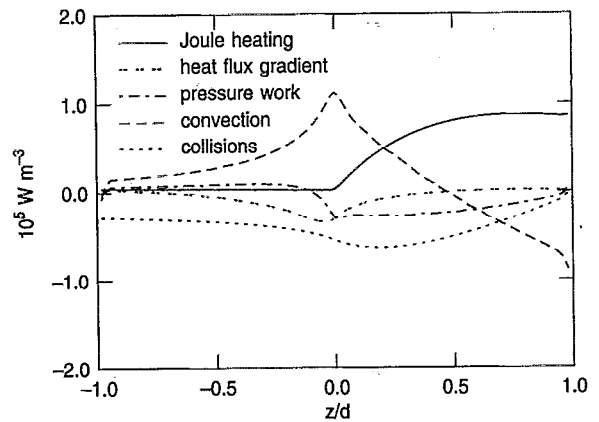


FIG. 5. Energy balance with forward scattering.

visible as the sharp minimum in the pressure gradient at  $z=0$ .

In Fig. 3, the collisional friction term is negative everywhere in the discharge, as expected. The individual components of the friction force [Eq. (20)] are plotted in Fig. 4. The ionization drag dominates the overall friction force, consistent with the high electron inertia. As an artifact of the pure forward-scattering model, the two electrons leaving the ionization collision have more momentum on the average than the incoming electron, resulting in a net momentum gain from ionization scattering.

It is possible to rewrite the closure relation for the friction, Eq. (34), in terms of the ionization and excitation cross sections [elastic collisions are ignored in the forward-scattering case and Fig. 2(c) shows that the average energy everywhere in the CF is higher than the inelastic thresholds]. However, the excess momentum of colliding electrons [Eqs. (18) and (19)] is difficult to incorporate into Eq. (34). Furthermore, the kinetic energy of the bulk electron motion points to a very anisotropic distribution function (see also Fig. 8 below). Therefore, the drift-diffusion approximation to the momentum balance [Eq. (35)] is clearly inappropriate under forward-scattering conditions.

Beam models appear more appropriate for forward-scattered electrons in the CF.<sup>12</sup>

We now turn to the energy balance, Eq. (24), and examine the behavior of the total energy profile shown in Fig. 2(c). (For forward-scattered electrons, the axial energy is synonymous with total energy.) Figure 5 shows the individual terms of Eq. (24) as a function of position. [The sign of the individual terms in Eq. (24) is carried with the term, e.g., "axial heat flux gradient" refers to  $-dq_z/dz$ .] In the high-field region close to the cathode ( $z=d$ ), Joule heating is the only source of energy, balancing convective energy transport away from the cathode. The convected energy from the cathode is the major source of energy in the NG. As the density of electrons builds up toward the CF-NG boundary, the collision rate increases (Fig. 2) and the collisional energy loss becomes the dominant loss mechanism. Collisional loss of energy is due mostly to the energy absorbed by newly created electrons except close to the anode where the average energy is low (Fig. 2) and ionization potential loss is the dominant energy sink.

Figure 6 shows the heat flux,  $q_z$ , from Eq. (25), as a function of position in the discharge. Qualitatively, the agreement with the temperature profile in Fig. 2(c) is good;  $q_z$  is small and positive in the CF (small electron-

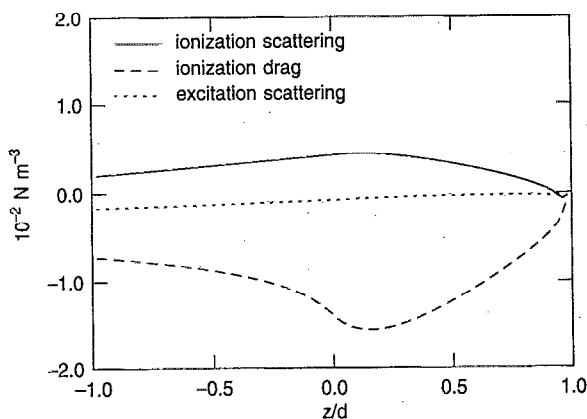


FIG. 4. Constituents of dynamical friction.

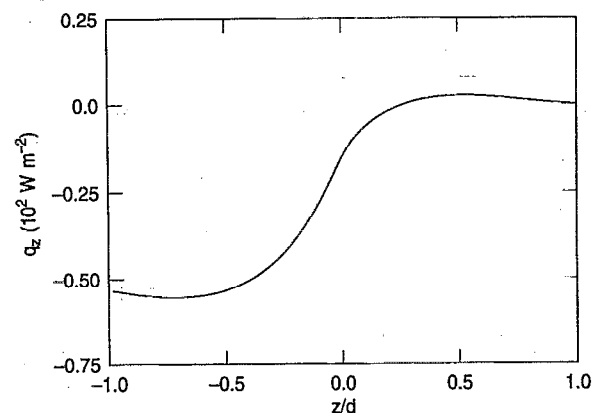


FIG. 6. Random heat flux profile in the discharge (forward scattering).

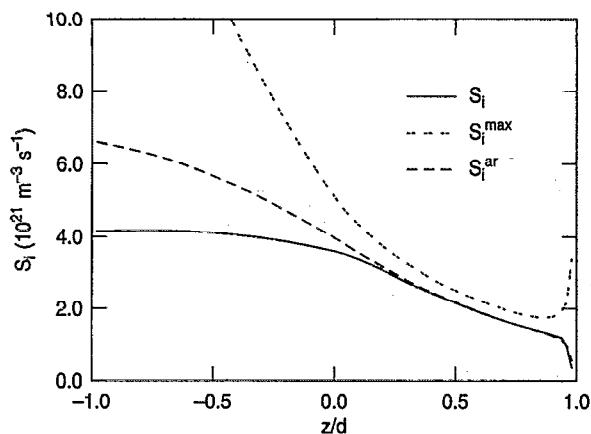


FIG. 7. Ionization rate from simulation (forward scattering) and from Arrhenius kinetics.

density implies small thermal conductivity) and large and negative in the NG. However, since the EDF is very anisotropic, the expression for the  $K$  following Eq. (37) is not justified. In fact the calculated value of the thermal conductivity is a strong function of position, and does not follow  $K \propto nT_z^{1/2}$ . The nonequilibrium EDF results in negative thermal conductivity over a significant fraction of the gap length. Given the strongly anisotropic EDF, deviation of the heat flux from the classical description is not surprising.

The ionization rate is compared to Arrhenius rate  $S_i^{Ar}$ , calculated using the value of the ionization cross section for  $\sigma_{eff}$  in Fig. 7. We use the average total energy as the characteristic energy:  $\bar{\epsilon} = \frac{1}{2}mu^2 + \frac{1}{2}kT_z$  (from Fig. 2, it is unreasonable to ignore the kinetic energy of the bulk motion in this system). It is somewhat unexpected that the two curves appear to agree more in the highly nonequilibrium CF than in the low-field NG region. In Fig. 8 we show the electron energy distribution function (EEDF) at two different positions, corresponding to the CF ( $z/d = 0.5$ ) and NG ( $z/d = -0.5$ ) regions. It is apparent from the figure that the distribution in the CF has little equilib-

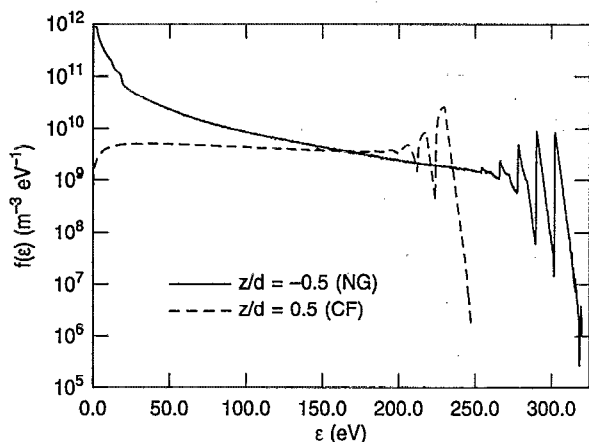


FIG. 8. EEDF at two positions in the discharge.

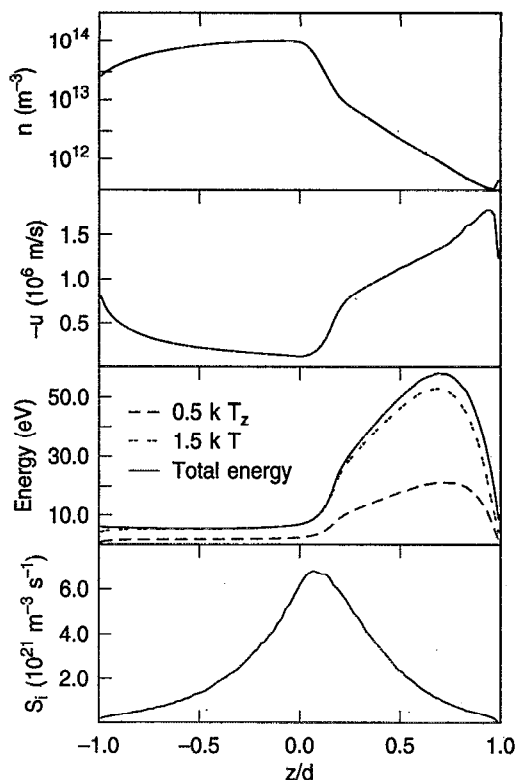


FIG. 9. Cathode fall properties using isotropic scattering model.

rium character. The reason for the good agreement between  $S_i$  and  $S_i^{Ar}$  is that both are close to  $S_i^{max}$ , because the average electron energy in the CF is much greater than the ionization potential [Fig. 2(c)]. In the NG, the average electron energy is not as high as in the CF. While Fig. 7 shows that the Arrhenius approximation overestimates the ionization rate in the NG, by 60% near the anode, the agreement is quite good overall.

## VI. ISOTROPIC SCATTERING

We now present results from a simulation in which the electrons scatter isotropically off the neutrals after each collision. Compared to forward scattering, isotropic scattering results in a much higher electron current gain in the CF (the ratio of electron current at the CF-NG boundary,  $z=0$ , to that at the cathode,  $z=d$ , is 23, compared to 3.4 for forward scattering). This is due to the cumulatively longer paths traversed by the electrons in the CF when they are scattered isotropically.

Figure 9 shows the same moments of the EDF that were shown for forward scattering in Fig. 2. It is clear that the effect of the isotropic scattering is greatest in the NG, where the density and average velocity profiles are qualitatively different in the two figures. The absorbing anode causes the average velocity in Fig. 9(b) to increase in magnitude from the CF-NG boundary ( $z=0$ ) to the anode ( $z=-d$ ), with a corresponding decrease in the density in Fig. 9(a). The density profile appears less sensitive to the anode than the average velocity profile because the anode-

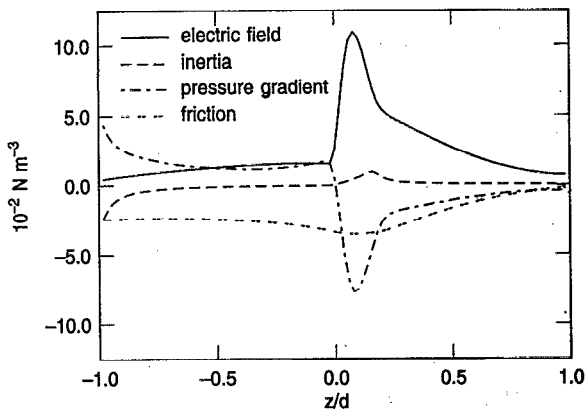


FIG. 10. Momentum balance with isotropic scattering.

induced decrease in density is partially offset by an increase in the flux due to ionization.

While the profiles in the CF from Figs. 2 and 9 are qualitatively similar, there are interesting differences. The minimum in the density (and the corresponding maximum in the average velocity) is closer to the cathode when the electrons are scattered isotropically. This is expected since isotropic elastic collisions cause complete loss of momentum on the average [Eq. (21)] and the drift velocity is determined more by the local-field value than by the inertial effects which dominate the forward-scattered electrons. The average electron energy also peaks closer to the cathode in Fig. 9(c) than in Fig. 2(c) because isotropic collisions allow more electrons to gain the requisite energy for inelastic collisions closer to the cathode. There is a sharp increase in the density and a corresponding drop in the average velocity near  $z/d=0.2$ . This is caused by backscatter from the low-field NG region, and takes the form of a pressure gradient in the momentum balance (see below). Comparison between the ionization rate in Fig. 2(d) to that in Fig. 9(d) shows that isotropic scattering causes the ionization rate to be sharply peaked at the CF-NG boundary due to a lower average energy in the NG [Fig. 9(c)].<sup>18</sup> Figure 9(c) also shows that the kinetic energy of bulk motion is small when electrons are scattered isotropically.

As before, it is instructive to quantify the above discussion by examining the terms of the conservation equations. In Fig. 10, we show the terms of the momentum balance [Eq. (14)]. The inertia term in Fig. 10 is negligible since the effect of isotropic collisions is to destroy all gained momentum. This is true even in the high-field region close to the cathode, in contrast to the arguments presented in Ref. 7. In the CF, the field acts to overcome the retarding effect of collisions as backdiffusion. The sharp drop in the average velocity visible near the sheath edge [ $z/d=0.2$  in Fig. 9(b)] is caused by the very negative pressure gradient. This represents the dilution of the beam created in the CF by the NG electrons diffusing against the field into the CF. The flow of electrons in the NG is driven by the field as well as by diffusion (the reversed pressure gradient).

We expect in the isotropic scattering case to justify the

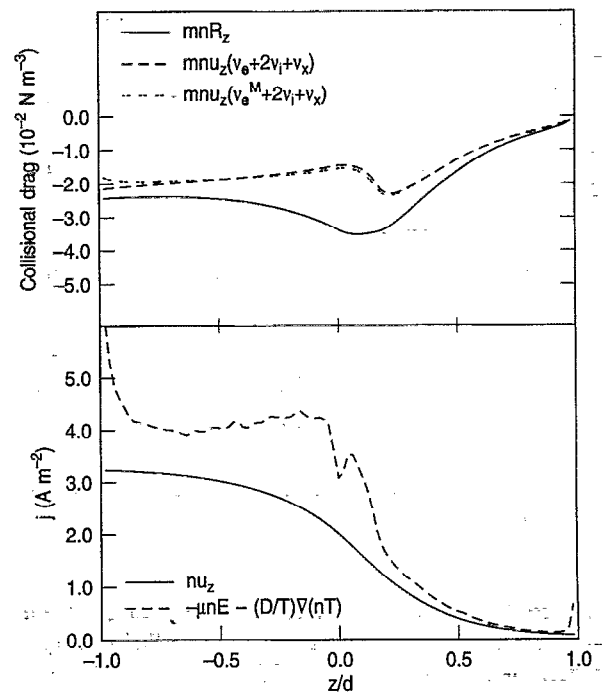


FIG. 11. Evaluation of mobility and drift-diffusion approximations: (a) friction force; (b) electron flux.

use of the electron mobility concept to describe the dynamical friction force. However, several modifications of the model considered earlier are necessary. With reference to Eq. (34), a breakdown of the collisional drag force reveals that for the cross-section set used here the friction, while dominated by elastic collisions, does have significant contributions from ionization and excitation (up to 30% near the sheath edge,  $z=0$ ). Therefore, it is necessary to include the inelastic collisions in the expression for the friction. Equation (34) is thus modified to read

$$mnR_z = mnn_g \langle v_z v (\sigma_e + \sigma_i + \sigma_x) \rangle + mu_z S_i \approx mnu_z (v_e + 2v_i + v_x), \quad (38)$$

where the assumption regarding the dominance of elastic collisions has been dropped and ionization drag has been explicitly included. In order to test the approximation, we must explicitly calculate the inelastic collision frequencies,  $v_i$  and  $v_x$ . This can be achieved through an Arrhenius description of inelastic rates; however, the error of the two approximations is then compounded. Inelastic rates are discussed separately below. For now, we proceed on the basis that the inelastic rates can be obtained through a particle simulation, and test the approximation by extracting the rates directly from the Monte Carlo results. In Fig. 11(a), we show the true dynamical friction term from the Monte Carlo simulation along with the curve calculated according to the right-hand side of Eq. (38). All collision frequencies, including elastic, have been obtained from the simulation. Also shown in the figure is a curve calculated by assuming that the elastic collision frequency can be cal-

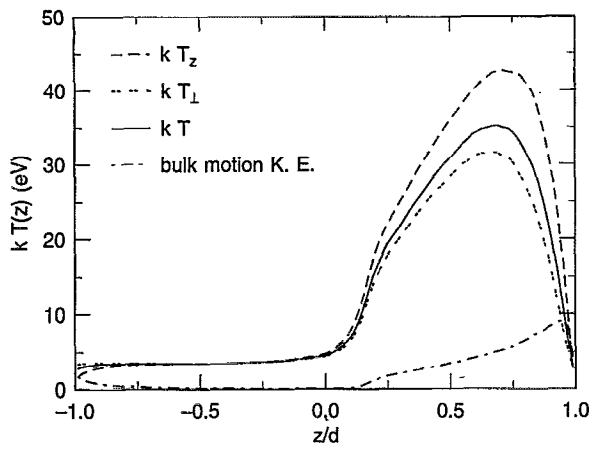


FIG. 12. Magnitudes of axial and perpendicular temperatures and energy of bulk motion.

culated according to a Maxwellian distribution; the temperature used to calculate this curve is obtained from the simulation.

Figure 11(a) shows that describing elastic collision rates by Maxwell-Boltzmann kinetics introduces a small additional error compared to that introduced by the mobility approximation itself. The approximate expression for the frictional force underestimates the magnitude of the force in the CF; apparently the quantities  $v$  and  $v_z$  are correlated in the electron beam traversing the CF and this correlation is neglected when  $\langle v_z v \sigma \rangle$  is approximated by  $u_z \langle v \sigma \rangle$ . (Ignoring threshold effects, the term  $\langle v_z v \rangle$  can be written as the sum of  $u_z \langle v \rangle$  and  $\langle w_z v \rangle$ . If the velocity distributions in the three coordinate directions are independent of each other, then  $\langle w_z v \rangle = \langle w_z \rangle \langle v \rangle = 0$ , which is the assumption made in defining the mobility. The additional assumption regarding the Maxwellian then consists of substituting  $\sqrt{8kT/\pi m}$  for  $\langle v \rangle$ .) In particular, the approximation appears to break down near the sheath edge where the true and approximated friction profiles are qualitatively different, in the region where the average velocity and the density profiles are greatly affected by the diffusive flux from the NG [Fig. 9(b)]. In the NG, the mobility approximation results in a collisional drag that increases towards the anode, in contrast to to the actual collisional drag.

Since in Fig. 10 the inertia term is small everywhere, it seems that the drift-diffusion equation (35) should apply. However, in keeping with the preceding paragraph, the expression for the mobility in Eq. (36) must be modified to include the inelastic rates. The modified mobility is calculated as

$$\mu = \frac{e}{m(\nu_e + 2\nu_i + \nu_x)} \quad (39)$$

and substituted into Eq. (35). The flux thus calculated is compared to the true flux from the Monte Carlo simulation in Fig. 11(b). The deviation between the curves in Fig. 11(b) mirrors the deviation in the friction curves in Fig. 11(a), with the largest deviation occurring near the sheath edge ( $z=0$ ). The effect of the artificial increase in the fric-

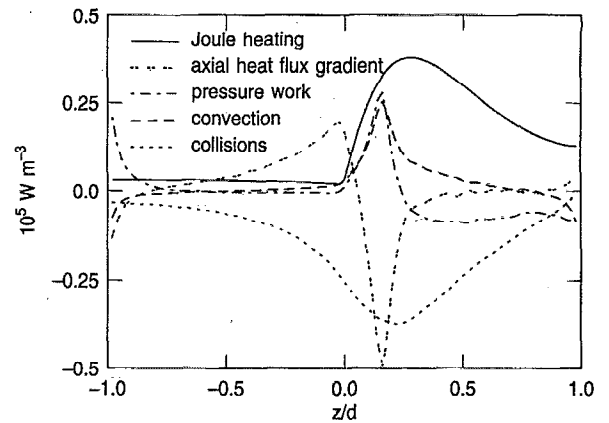


FIG. 13. Axial energy balance with isotropic scattering.

tion force through most of the NG due to the mobility approximation is visible in the artificially decreasing flux in the NG predicted by the drift-diffusion model.

The energy of electrons that are isotropically scattered is characterized by two temperatures,  $T_z$  and  $T_\perp$ . Figure 12 shows these temperature profiles, as well as that of the average temperature  $T$ . Also shown on the figure is the quantity  $mu_z^2/k$ , which represents the energy of the bulk motion. It is apparent from the figure that the latter is small. Figure 12 also shows that  $T_z$  is substantially larger than  $T_\perp$  in the CF due to the field. Figure 12 provides a quantitative estimate of the error introduced into a fluid description by writing  $P_{zz}$  as  $nkT$  instead of as  $nkT_z$ ; inside the CF (where  $n$  is small) the error is about 20%, whereas in the NG (large  $n$ ) the two temperatures are very close. A separation of  $T$  and  $T_z$  induced by the adsorbing anode is also visible in the figure.

These temperatures are determined by separate energy balance equations. We consider the axial energy balance [Eqs. (24) for  $T_z$ ] and the total energy balance [Eq. (29) for  $T$ ].  $T_\perp$  can be obtained from  $T_z$  and  $T$ . The various terms of Eqs. (24) and (29) are plotted in Figs. 13 and 14, respectively. Comparison between the two figures shows

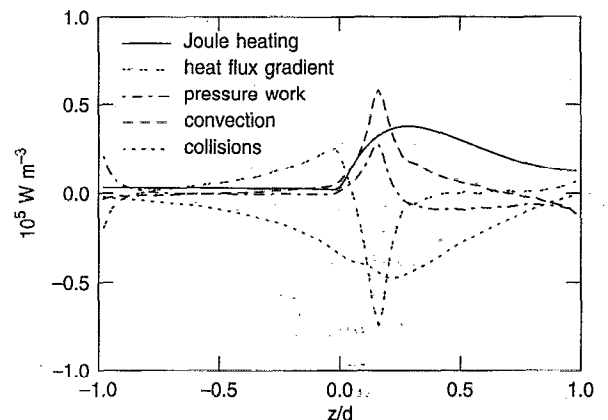


FIG. 14. Total energy balance with isotropic scattering.

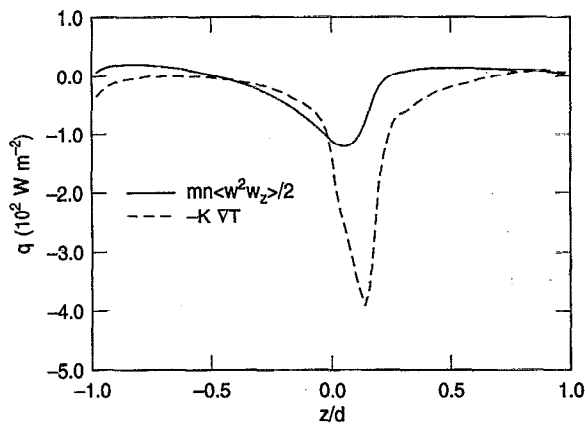


FIG. 15. Heat flux profile in the discharge (isotropic scattering) from simulation and thermal conduction approximation.

that they are qualitatively similar; given the similar profiles for  $T$  and  $T_z$  in Fig. 12, this is expected.

The collisional loss of energy is negative everywhere in Figs. 13 and 14, as expected. Resolution of this term according to Eq. (27) for Fig. 13 reveals that the excitation loss is small compared to ionization and the loss to the perpendicular direction. The latter is dominated by elastic scattering. Note that elastic scattering is significant in the axial energy balance, but negligible in the total energy balance [Eq. (31)]. The makeup of the collisional loss in Fig. 14 is dominated by the ionization term in Eq. (31). The ionization loss is due, as in Fig. 13, to the random energy gained by the new electron (in the CF) as well as the potential energy loss to the neutral (in the NG).

In Figs. 13 and 14, there is an interchange of energy transport mechanisms between the pressure work and energy convection on one hand, and the heat flux gradient on the other hand, near the sheath edge ( $z/d \approx 0.2$ ). On the NG side of the CF-NG boundary ( $z=0$ ), the heat flux gradient is the dominant source of energy except near the anode.

The energy balance equation is usually closed by assuming that the random heat flux follows classical heat conduction theory. The applicability of the heat conduction Eq. (37) is examined by plotting the heat flux thus obtained and comparing it to the actual heat flux from the simulation. The thermal conductivity used to generate the plot is based upon the modified mobility, Eq. (39). The results are shown in Fig. 15. It is clear that the use of classical heat conduction theory results in a poor approximation to the actual heat flux. While both curves have minima near the sheath edge, the classical theory overestimates the heat flux by a factor of 4 in that region. This could be the result of the particular scaling value used for  $K$ , although the factor of  $\frac{5}{2}$  used in the expression relating  $K$  and  $D$  in Refs. 5 and 7 instead of the  $\frac{3}{2}$  used here worsens the discrepancy observed. Also, in a large part of the CF heat flux is positive and flowing against the temperature gradient; this effect is outside the scope of the fluid description.

Finally, we examine the ionization rate in terms of the

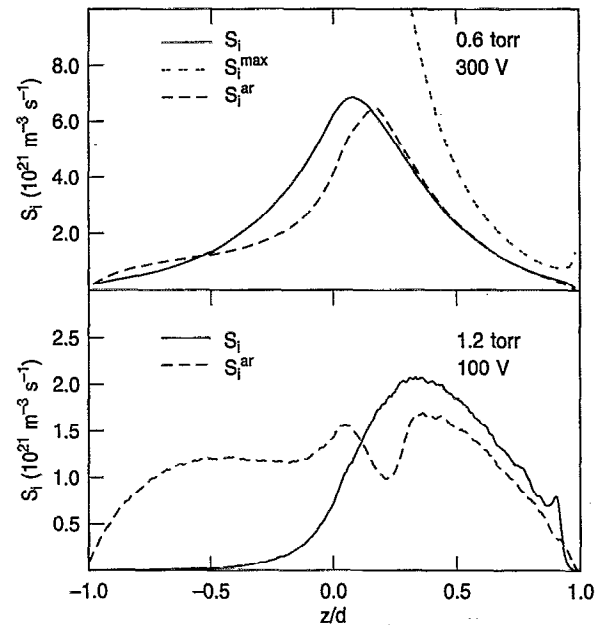


FIG. 16. Ionization rate from simulation (isotropic scattering) and from Arrhenius kinetics.

Arrhenius rate model developed in the previous section. Figure 16(a) shows the ionization rate from Fig. 9(d), as well as the calculated Arrhenius rate  $S_i^{Ar}$ , from Eq. (32) and (33). Here,  $\bar{\epsilon} = kT$ . Also shown is the maximum ionization rate based on the pre-exponential factor,  $S_i^{max}$  from Eq. (33). As in the forward-scattering case,  $S_i^{Ar}$  agrees with  $S_i$  in the CF when both are close to  $S_i^{max}$ . In the NG, the average energy of the electrons is significantly lower when they are scattered isotropically than when they are forward scattered. This decreases the value (and increases the importance) of the Boltzmann factor from  $O(0.5)$  for the forward-scattering case (Fig. 7) to  $O(0.01)$  for isotropic scattering. Therefore the agreement between  $S_i^{Ar}$  and  $S_i$  in the NG to within a factor of 2 is surprisingly good, given the non-Maxwellian EDF. Near the anode, the Boltzmann factor overpredicts the tail of the EDF; this is due to the absorbing anode which creates a one-sided velocity distribution.

Figure 16(a) shows the ionization rate to be single peaked, in contrast to the rates shown in Refs. 5 and 7 which are double peaked. The double-peaked rate predicted by fluid models is believed to be an artifact of the Arrhenius description of the rate in which two separate terms, one representing the density (high in the NG) and the other the temperature (high in the CF), are multiplied to obtain the composite rate. In reality, the high-energy tail of the distribution which enters the NG from the CF is responsible for the ionization. Evidence of an artificial double peak is visible in Fig. 16(b), where we show for a different set of conditions, the ionization rate obtained from the simulation and the double-peaked Arrhenius description of the same rate. It should also be noted that the double-peaked ionization rate is predicted only by fluid models that use the Arrhenius description.<sup>5,7</sup> Inelastic rate

profiles from previous Monte Carlo studies and experimental measurements do not show two peaks.<sup>12,15,19</sup> A two-fluid model to represent separately the "hot" fluid from the CF and the "cold" fluid in the NG may yield more physical results.

## VII. CONCLUSIONS

We have calculated all the terms of the first and second moments of the Boltzmann equation for electron transport in a dc glow under a specified electric field, using a Monte Carlo particle simulation. Two extreme scattering mechanisms, pure forward scattering and isotropic scattering, have been examined. The fluid analysis reveals that there are no common negligible terms in the moment equations for the two scattering cases, i.e., for realistic angular anisotropic scattering all terms need to be retained to capture the full physics. However, the equations may be simplified for the individual scattering mechanisms (e.g., electron inertia is negligible in the momentum balance under isotropic scattering).

A fluid description of electrons that are forward scattered is complicated by the resulting anisotropic distribution function. For this reason, it does not appear reasonable to treat forward-scattered electrons as a fluid since the mobility and heat conduction concepts do not apply. In spite of the non-Maxwellian EDF, however, ionization rates can be described to within 60% by Arrhenius kinetics. The kinetic energy of the bulk motion must be accounted for when electrons are forward scattered. Analysis of specific moments shows the maximum change in transport mechanisms (balance terms are largest) at the sheath edge.

Isotropic scattering leads to a more isotropic distribution and therefore to more "fluid" behavior. Transport mechanisms show the greatest changes some distance into the sheath. This is due to diffusion of low-energy electrons from the bulk plasma into the CF which causes dilution of the electron beam from the CF before the beam actually arrives at the low-field region. The gradients of the electron density, average velocity, and temperature all show sharp changes in this region reflecting the onset of the dilution. The ionization rate is not affected by this phenomenon, since it is dominated by the high-energy tail of the EDF.

Nevertheless, the Arrhenius description of the ionization rate is accurate to within a factor of 2 in the NG, and better in the CF. However, there is a possibility of obtaining a double-peaked inelastic rate profile as an artifact of this description. The mobility relation and the accompanying drift-diffusion approximation also produce results which are good to within a factor of 2. The closure relation for the heat flux is more troublesome, because classical

heat conduction overestimates the heat flux at the sheath edge by a factor of 4 and fails to account for kinetic effects (where the heat flows against the temperature gradient) in other parts of the discharge.

It is important to note that we have not solved a set of fluid equations. It is likely that since these equations are conservative, a self-consistent solution of these equations will distribute the errors found in the various approximations and result in a sound representation of the physical reality. Nevertheless, the results here indicate that discrepancies of 50%–100% between fluid and kinetic models of dc discharges should not be unexpected. Given errors in cross-section data near these magnitudes, the relative efficiency of fluid models may still make these worthwhile. It is also possible to increase the accuracy of fluid models by hybridizing them with kinetic methods.

- <sup>1</sup>M. Surendra and D. B. Graves, *IEEE Trans. Plasma Sci.* **PS-19**, 144 (1991).
- <sup>2</sup>C. K. Birdsall, *IEEE Trans. Plasma Sci.* **PS-19**, 65 (1991).
- <sup>3</sup>D. Vender and R. W. Boswell, *IEEE Trans. Plasma Sci.* **PS-18**, 725 (1990).
- <sup>4</sup>T. J. Sommerer, W. N. G. Hitchon, R. E. P. Harvey, and J. E. Lawler, *Phys. Rev. A* **43**, 4452 (1991).
- <sup>5</sup>D. B. Graves and K. F. Jensen, *IEEE Trans. Plasma Sci.* **PS-14**, 78 (1986).
- <sup>6</sup>M. S. Barnes, T. J. Cotler, and M. E. Elta, *J. Comput. Phys.* **77**, 53 (1988).
- <sup>7</sup>M. Meyyappan and J. P. Kreskovsky, *J. Appl. Phys.* **68**, 1506 (1990).
- <sup>8</sup>J. P. Boeuf, *J. Appl. Phys.* **63**, 1342 (1988).
- <sup>9</sup>T. J. Sommerer, M. S. Barnes, J. H. Keller, M. J. McCaughey, and M. J. Kushner, *Appl. Phys. Lett.* **59**, 638 (1991).
- <sup>10</sup>N. Sato and H. Tagashira, *IEEE Trans. Plasma Sci.* **PS-19**, 102 (1991).
- <sup>11</sup>J. P. Boeuf and L. C. Pitchford, *IEEE Trans. Plasma Sci.* **PS-19**, 286 (1991).
- <sup>12</sup>M. Surendra, D. B. Graves, and G. M. Jellum, *Phys. Rev. A* **41**, 1112 (1990).
- <sup>13</sup>K. H. Schoenbach, H. Chen, and G. Schaefer, *J. Appl. Phys.* **67**, 154 (1990).
- <sup>14</sup>A. C. Dexter, T. Farrell, and M. I. Lees, *J. Phys. D* **22**, 413 (1989).
- <sup>15</sup>E. A. Den Hartog, D. A. Doughty, and J. E. Lawler, *Phys. Rev. A* **38**, 2471 (1988).
- <sup>16</sup>T. J. Sommerer, W. N. G. Hitchon, and J. E. Lawler, *Phys. Rev. A* **39**, 6356 (1989).
- <sup>17</sup>M. Dalvie, S. Hamaguchi, and R. T. Farouki, *Phys. Rev. A* **46**, 1066 (1992).
- <sup>18</sup>J. P. Boeuf and E. Marode, *J. Phys. D.* **15**, 2169 (1982).
- <sup>19</sup>T. J. Moratz, *J. Appl. Phys.* **63**, 2558 (1988).
- <sup>20</sup>W. P. Allis, in *Handbuch der Physik*, edited by S. Flügge (Springer, Berlin, 1956), Vol. 21, p. 383.
- <sup>21</sup>K. Miyamoto, *Plasma Physics for Nuclear Fusion* (MIT Press, Cambridge, MA, 1980).
- <sup>22</sup>R. T. Farouki, S. Hamaguchi, and M. Dalvie, *Phys. Rev. A* **44**, 2664 (1991).
- <sup>23</sup>R. B. Bird, W. E. Stewart, and E. N. Lightfoot, *Transport Phenomena* (Wiley, New York, 1960).
- <sup>24</sup>E. E. Kunhardt, *Phys. Rev. A* **43**, 6664 (1991), and references therein.
- <sup>25</sup>R. A. Gottscho, A. Mitchell, G. R. Scheller, N. L. Schryer, D. B. Graves, and J. P. Boeuf, *Electrochem. Soc.* **88-12**, 1 (1988).
- <sup>26</sup>N. A. Tran, E. Marode, and P. C. Johnson, *J. Phys. D* **10**, 2317 (1977).